Model Validation and Estimation of the Complete Carbon Cycle in the Northeastern United States

Shaun Howe

A scholarly paper in partial fulfillment of the requirements for the degree of

Master of Science

May 2019

Department of Atmospheric and Oceanic Science
University of Maryland
College Park, Maryland

Advisor: Dr. Ning Zeng

Table of Contents

Abstract

To obtain accurate greenhouse gas emissions estimates, it is important to understand the influence of the biosphere on atmospheric carbon dioxide (CO_2). This is difficult as observations are sparse over large spatial domains. The Northeastern United States is an area of interest for studying the carbon cycle because it is highly urbanized but also contains an active biosphere. To study the influence of the biosphere on CO_2, the VEgetation-Global-Atmosphere-Soil (VEGAS) model is used alongside the Weather Research and Forecasting model with coupled Chemistry (WRF-Chem). VEGAS model output is first assessed against observations and other CO_2 analyses for the Northeast Corridor of the United States for the period of November 2016 through October 2017. Biological fluxes from VEGAS are then utilized in the WRF-Chem modeling framework along with anthropogenic CO_2 emissions to simulate atmospheric CO_2. Results show that the VEGAS model underestimates the length of the growing season and the magnitude of the diurnal cycle in biospheric productivity. The model does capture the spatial distribution in biological fluxes in the Northeast. Simulated CO_2 from WRF-Chem matches observations well in urban areas but does not match observations in rural areas where biological uptake dominates the diurnal cycle in CO_2. Biological uptake is estimated to sequester 32% of anthropogenic emissions in the innermost model domain over Washington DC/Baltimore, Maryland area.

Acknowledgements

I would like to thank my advisor Professor Ning Zeng and Professor Russell Dickerson for guiding me through the research process. I would also like to thank Cory Martin for being my "unofficial" advisor and teaching me so much about research and the modeling system used for this work. I would like to thank NIST for funding my research. More specifically, I would like to thank the team at NIST including Sharon Gourdji, James Whetstone, Anna Karion, Israel Lopez-Coto, David Allen, Kimberly Mueller, and Tamae Wong for their advice and guidance. Lastly, I would like to thank my family, girlfriend, and friends for keeping me motivated during my time at the University of Maryland. I wouldn't have been able to do it without their support.

List of Tables

List of Figures

List of Symbols/Acronyms

AWOS - Automated Weather Observing System

ARL - Arlington, VA carbon dioxide tower site

BC - Boundary Condition

BUC - Bucktown, MD carbon dioxide tower site

CO_2 - carbon dioxide

$[CO_{2_{Anth}}]$ - anthropogenic carbon dioxide concentration tracer

$[CO_{2_{Bio}}]$ - biospheric carbon dioxide concentration tracer

$[CO_{2_{Total}}]$ - total carbon dioxide concentration tracer

CF_{har} - carbon flux from harvested and decaying wood

CF_{fire} - carbon flux from fire

CF_{ta} - carbon flux to the atmosphere

CT-NRT - CarbonTracker Near Real-Time

CRUNCEP - blended CRU and NCEP Reanalysis temperature record

D01 - outermost WRF-Chem modeling domain

D02 - intermediate WRF-Chem modeling domain

D03 - innermost WRF-Chem modeling domain

DGVM - Dynamic Global Vegetation Model

EPA - Environmental Protection Agency

FFDAS - Fossil Fuel Data Assimilation System

$F(CO_2)_{CT-NRT}$ - initial and boundary conditions of atmospheric carbon dioxide from the CT-NRT product

$F(CO_2)_{FFDAS}$ - flux of carbon dioxide from the FFDAS emissions inventory

$F(CO_2)_{VEGAS}$ - flux of carbon dioxide from the VEGAS vegetation model

GPP - Gross Primary Productivity

HAL - Halethorpe, MD carbon dioxide tower site

HYDE - History Database of the Global Environment

US-IB2 - AmeriFlux flux tower site at the Fermi National Laboratory, IL

IC - Initial Condition

JES - Jessup, MD carbon dioxide tower site

KCGE - Cambridge-Dorchester Regional Airport

KDMW - Carroll County Regional Airport

LAI - Leaf Area Index

LEW - Lewisburg, PA carbon dioxide tower site

NARR - North American Regional Reanalysis

NDVI - Normalized Difference Vegetation Index

NIST - National Institute of Standards and Technology

NEB - Northeast Baltimore, MD carbon dioxide tower site

NEC-B/W - Northeast Corridor - Baltimore/Washington DC

NEE - Net Ecosystem Exchange

NEP - Net Ecosystem Production

PBL - Planetary Boundary Layer

PFT - Plant Functional Type

TMD - Thurmont, MD carbon dioxide tower site

TRENDY - model intercomparison to determine the trends in net land carbon exchange

UNY - Utica, NY carbon dioxide tower site

R_a - autotrophic respiration
R_{es} - total respiration from the soil
R_h - heterotrophic respiration
R_h - soil heterotrophic respiration
SNPP - Suomi National Polar-orbiting Partnership
SNP - Shenandoah National Park, VA carbon dioxide tower site
VEGAS - VEgetation-Global-Atmosphere-Soil model
VIIRS - Visible Infrared Imaging Radiometer Suite
WD - Wind Direction
WRF-Chem - Weather Research and Forecasting model with coupled Chemistry
WS - Wind Speed

Chapter 1. Introduction

After decreasing for 3 straight years, carbon dioxide (CO_2) emissions from US power plants rose 0.6% in 2018 to 1.93 GtC per year (EPA 2019). The rise in emissions is a result of increased power demand associated with a thriving US economy and inexpensive oil. This news comes at a troubling time as recent research from the IPCC states that we may have as little as 12 years to keep global mean surface temperature warming below 1.5°C by the end of the century (Masson-Delmotte et al. 2018). To inform decisions on controlling CO_2 emissions, it is essential to have proper estimates of atmospheric CO_2 concentrations. Since the late 1950s, atmospheric observations of CO_2 have been made at Mauna Loa in Hawaii to monitor earth's climate (Keeling et al. 1976). These stations have expanded into the Greenhouse Gas Reference Network which combines tower, balloon, aircraft, and ship measurements to provide high quality observations of CO_2 globally (Masarie et al. 2014). Observations from the Greenhouse Gas Reference Network are used in different modeling frameworks to estimate anthropogenic sources and create gridded CO_2 analyses (Patra et al. 2005; Peylin et al. 2005; Peters et al. 2007; Gurney et al. 2008; Rayner et al. 2008; Chevallier et al. 2010; Maki et al. 2010; Niwa et al. 2012). Despite the growth of the global network, smaller, more regional, networks of observations are needed to understand emissions on a finer spatial scale.

Multiple studies have been conducted using high density networks of CO_2 observations and high resolution modeling to constrain CO_2 emissions in cities (Briber et al. 2013; Kort et al. 2013; Lauvaux et al. 2013; Bréon et al. 2015; Turnbull et al. 2015; Feng et al. 2016; Lauvaux et al. 2016; Miles et al. 2017; Sargent et al. 2018). These

studies utilize both inverse modeling (top-down) and city-level emissions (bottom-up) methods to constrain CO_2 emissions estimates. For inverse modeling, background CO_2 measurements from observation towers outside of urban areas are necessary to understand the inflow of CO_2 into cities. Background towers tend to be in areas of high biological productivity. Fluxes between the biosphere and atmosphere provide a large source of uncertainty in inverse modeling frameworks when trying to understand the background state of CO_2. It is even more difficult to constrain the biosphere for bottom-up estimations due to a lack of data on vegetation at the city-level. In a comparison between top-down and bottom-up emissions estimates for Indianapolis, IN, the largest source of error between the two methods came from the biosphere. It was estimated that 0.58 – 1.17 MtC from the biosphere could reconcile the difference between the two methods over the eight-month study period in the dormant season (Gurney et al. 2017). These differences need to be minimized to provide more accurate estimations of atmospheric CO_2.

A recent network of observational towers operated by the National Institute of Standards and Technology (NIST) has been implemented over the Northeast Corridor centered on the Baltimore, MD and Washington, DC metropolitan areas (NEC-B/W) (Lopez-Coto et al. 2017; Mueller et al. 2018). The NEC-B/W is interesting to study because of the inherent complexities in the carbon cycle. The Northeastern US is the most highly urbanized area of the US and thus has a large anthropogenic signal. It is also highly vegetated with productive deciduous forests and is downwind of much of the nation's agriculture. North American forests are a net carbon sink with an uptake of 217 Tags per year (Domke et al. 2018). If all the carbon emitted from power plants from the

EPA estimate were taken up by the biosphere in North America, the biosphere would account for 12.5% of US emissions.

To understand the role of the biosphere over the NEC-B/W, a carbon cycle model is used in conjunction with a meteorological transport model. The carbon cycle model is first validated against in-situ observations, satellite observations, and another carbon dioxide analysis. Hourly fluxes from the carbon cycle model are used with the meteorological model along with anthropogenic fluxes to simulate the carbon cycle in its entirety. These results are compared to NEC-B/W CO_2 observation towers to assess the accuracy of WRF-Chem in simulating the carbon cycle and to understand the role of the biosphere in counteracting anthropogenic CO_2 emissions.

Chapter 2. Data

This chapter describes the two types of data used in this analysis: input data for initializing and running the model (Section 2.1.1 and Section 2.1.2) and data used to validate the output from the two models (Section 2.1.1 and Section 2.2).

2.1 Gridded CO_2 Datasets

2.1.1 CarbonTracker Near Real-Time

The CarbonTracker Near Real-Time (CT-NRT) product is a CO_2 analysis which utilizes a transport model, a biosphere model, and data assimilation to generate a global CO_2 product at a 1° x 1° horizontal resolution and three-hourly temporal resolution (Peters et al. 2007). The CT-NRT product estimates CO_2 fluxes and CO_2 concentrations. To estimate biological fluxes, CT-NRT uses the CASA (Carnegie-Ames-Stanford Approach) Model to estimate mean Net Ecosystem Production (NEP) (Potter and Klooster 1997). This diagnostic biosphere model uses satellite derived Normalized Difference Vegetation Index (NDVI) data, described in Section 2.2.1, to drive biosphere fluxes.

The CT-NRT product also provides gridded atmospheric CO_2 mole fraction data. CT-NRT provides three-dimensional mole fractions of CO_2 at a 1° x 1° horizontal resolution and three-hourly temporal resolution.

2.1.2 FFDAS

Fossil fuel emissions data for this study comes from the Fossil Fuel Data Assimilation System (FFDAS) (Rayner et al. 2010). The system utilizes the Kaya identity to aggregate fossil fuel emissions based on population and economic data for a given region. Night lights data are assimilated into the system to constrain errors in the Kaya

identity. Emissions in FFDAS are provided at an hourly temporal resolution and a spatial resolution of 0.1° x 0.1° for the year of 2015. There are likely differences in emissions between 2015 and 2017 which is the year used in this analysis. FFDAS was found to have a high bias when compared to tower observations in the NEC-B/W region for February 2015 (Martin et al. 2019).

2.2 Observations

2.2.1 VIIRS NDVI

The Suomi Polar-Orbiting Partnership (SNPP) is a polar orbiting satellite operated by the National Oceanic and Atmospheric Administration. It orbits the earth 14 times daily and was launched in October 2011. One of the principal instruments for imaging the land and atmosphere onboard the satellite is the Visible-Infrared Imaging Radiometer Suite (VIIRS). The instrument is a whiskbroom scanning radiometer that images the earth in the visible and infrared bands. These bands are used to calculate remotely sensed metrics of biological productivity. One such metric is the Normalized Difference Vegetation Index (NDVI). NDVI is calculated from imagery bands I2 (near-infrared: $0.846 - 0.855$ μm) and I1 (visible: 0.600-0.680 μm) (Kogan et al. 2015).

$$NDVI = \frac{I2 - I1}{I2 + I1} \text{ (1)}$$

Vegetation reflects radiation in the near-infrared and absorbs in the visible. The NDVI data used in this analysis has a spatial resolution of 4 km and has a weekly temporal resolution (Yang et al. in press).

2.2.2 AmeriFlux

The AmeriFlux observation network has provided biosphere/atmosphere fluxes of CO_2, water vapor, and energy for over 90 stations in various regions in the United States

since 1996 (Baldocchi et al. 2018). AmeriFlux tower sites use sonic anemometers to measure three-dimensional wind velocities and virtual temperature as well as sensors to measure water vapor and CO_2. Fluxes are calculated using meteorological measurements and gas concentrations by the eddy covariance method. The station that is used for this comparison is US-IB2 (Latitude: 41.8406200; Longitude: -88.2410300) which is located at Fermilab outside of Chicago, IL (Matamala).

2.2.3 NIST Tower Network

A network of 16 observation sites is planned for the NEC-B/W project to provide in-situ measurements of CO_2. These measurements will be used for top-down analyses of emissions using different inversion frameworks. There are currently 13 sites already collecting observations. Each site contains a state of the art Cavity Ring-Down Spectrometer managed by Earth Networks. The observational system is identical to that used in the Los Angeles Megacities project (Verhulst et al. 2017). Many of the sites have 2 inlets at different heights for calculating CO_2 gradients. The height of the inlets varies depending on tower location. A list of the towers used in this analysis can be found in Table 1 and locations of the tower sites are mapped in Figure 1.

Table 1. *A list of CO_2 observation sites used to compare to WRF-Chem output. Sites designated as background are in rural areas which are influenced by the biosphere. Urban sites are in urban areas and are influenced by anthropogenic emissions.*

Site Code	Location	Site Type
LEW	Lewisburg, PA	Background
UNY	Utica, NY	Background
SNP	Shenandoah National Park, VA	Background
BUC	Bucktown, MD	Background
TMD	Thurmont, MD	Background
ARL	Arlington, VA	Urban
NEB	Northeast Baltimore, MD	Urban
JES	Jessup, MD	Urban
HAL	Halethorpe, MD	Urban

2.1.4 Airport Meteorological Observations

Automated Weather Observing Systems (AWOS) take meteorological observations at regional airports around the US. These stations are regulated by the Federal Aviation Administration and managed by state and local governments. AWOS stations measure wind speed (WS), wind direction (WD), temperature, humidity, dew point, pressure, cloud height, visibility, and precipitation as well as estimate present weather conditions and runway conditions. Wind speed and direction data from the Cambrige-Dorchester Regional Airport (KCGE Latitude: 38.5393; Longitude: -76.0304) and Carroll County Regional Airport (KDMW Latitude: 39.6083; Longitude: -77.0077) AWOS stations are used in this study. The sensors used to measure wind speed and direction have an accuracy within 2 knots and $\pm 5°$ (FAA 2017). The wind speed and direction data used in this analysis are provided every 20 minutes.

Chapter 3. Methods

The chemical transport model used in this analysis is the Weather Research and Forecasting Model with coupled Chemistry (WRF-Chem) (Grell et al. 2005; Skamarock et al. 2008; Beck et al. 2011). Anthropogenic emissions data along with biological flux data from the VEgetation-Global-Atmosphere-Soil (VEGAS) model provide CO_2 sources and sinks at the surface in the WRF-Chem modeling framework (Zeng et al. 2005). This modeling framework is the same system used in Martin et al. 2019 with some slight differences. For this simulation, carbon fluxes from the biosphere are provided to WRF-Chem in an offline framework instead of an online approach. This is to ensure a better representation of the biosphere through proper spinup and driver meteorological data. A simulation of VEGAS is performed and analyzed for the period of November 1st, 2016 through November 1st, 2017. This period is chosen to coincide with other inverse modeling studies over the same domain. VEGAS output is validated against VIIRS NDVI, the US-IB2 AmeriFlux site, and the CT-NRT product at the diurnal and seasonal scales to better understand vegetation during the growing season in NEC-B/W.

Using biological fluxes from VEGAS and anthropogenic fluxes from FFDAS, a forward simulation of WRF-Chem is performed for July 2, 2017 through July 9, 2017. The model is analyzed for the period of July 3, 2017 through July 9, 2017 to allow for one day of mixing in the model. Total CO_2 output from the WRF-Chem run is validated against observational towers in the region. The contribution of the biosphere to the uptake of anthropogenic emissions is further examined through the WRF-Chem tracer experiment.

3.1 VEGAS Modeling

VEGAS is a Dynamic Global Vegetation Model (DGVM) that uses prognostic equations to simulate the growth of 5 vegetation carbon pools and 6 soil carbon pools using driver meteorological data. To simplify vegetation growth in a numerical modeling framework, vegetation models bin plants by their productivity using Plant Functional Types (PFTs). Vegetation is modeled using 5 PFTs which include broadleaf, needle leaf, cold grass, warm grass, and cropland. Photosynthesis is simulated using a method similar to Collatz et al. 1992. This technique uses a co-limiting factor to allow gradual responses in individual components of the model. Photosynthesis is controlled by temperature, soil moisture, light, and CO_2 dependent growth factors. Competition between trees and grass is simulated in the model through the light dependent factor, which is a function of PFT-height and Leaf Area Index (LAI) (Zeng et al. 2005).

VEGAS must to be run for 300 years to allow for the carbon pools to build up. This is because the model does not use prior biological information and thus the carbon pools must be solved dynamically from a zero state. This is known as model spinup. We use the TRENDY model protocol for model spinup (Sitch et al. 2015). First, the model is run hourly for 300 years without land use at a 2.5° x 2.5° spatial resolution. The restart files are then used to initialize the model for another 300-year simulation with land use at the same spatial and temporal resolution. For this simulation, land use was kept constant by utilizing the land use information for the year 2000 for simplicity. A summary of the input data used to run VEGAS is provided in Table 2. The vegetation variables from VEGAS that are used in this analysis are listed in Table 3.

Table 2. *Input data used to run VEGAS.*

Input Data	Dataset	Horizontal Resolution	Temporal Resolution	Citation
2-m Temperature	CRUNCEP	1° x 1°	6-hourly	(Viovy 2019)
Land Use History	HYDE 3.2	0.5° x 0.5°	yearly	(Klein Goldewijk et al. 2011)
Precipitation	CRU/ OPI/PRECL	0.5° x 0.5° (blended)	6-hourly	(Hulme et al. 1998; Janowiak et al. 1999; Chen et al. 2002)

The data products used to validate the VEGAS simulation include VIIRS NDVI data, CT-NRT biological fluxes, and AmeriFlux observations. Because of the large difference in resolution between the NDVI product and the vegetation model, 4 km compared to 2.5° x 2.5° or (~ 55 km), NDVI is spatially averaged over the outermost model domain and compared to spatially averaged NEP from VEGAS. This provides a comparison of the seasonality of biological productivity in the vegetation model.

Comparing VEGAS to CT-NRT is interesting because of the structural differences between these products, CT-NRT uses a diagnostic model for biological fluxes and VEGAS is a prognostic model. Spatial comparisons are made between VEGAS and CT-NRT during the growing season of 2017 while diurnal comparisons are performed between VEGAS and CT-NRT for July 2, 2017 through July 6, 2017.

Only one AmeriFlux site is used for comparison in this study to show the typical offset between VEGAS and the AmeriFlux observations at US-IB2. The site is also used to illustrate that both the model and observations show biological uptake as early as mid-March. Observations from US-IB2 are compared against biological uptake from the grid cell in the vegetation model corresponding to the location of US-IB2 in March of 2017.

Table 3. *The VEGAS flux variables used in this analysis. GPP (Gross Primary Productivity) is the rate at which plants produce organic compounds. R_a (autotrophic respiration) is the metabolism of organic matter by plants. R_h (heterotrophic respiration) is the metabolism of organic matter by bacteria, fungi, and animals. CF_{har} is the decay rate of harvested crop and wood. CF_{fire} is the release of carbon from wildfires.*

Flux Variable	Formula
Net Ecosystem Production (NEP)	$NEP = GPP - R_a - R_h$
Net Ecosystem Exchange (NEE)	$NEE = -NEP$
Carbon Flux to Atmosphere (CF_{ta})	$CF_{ta} = CF_{har} + CF_{fire} - NEP$

3.2 WRF-Chem Modeling

Figure 1 shows the three nested WRF-Chem model domains: D01 (outermost domain), D02 (intermediate domain), and D03 (innermost domain). The D01 domain contains almost the entire Northeastern and Mid-Atlantic United States and has a horizontal resolution of 9 km. The D01 domain extends into the Midwestern United States to capture upwind emissions from urban areas. This domain also includes the Corn Belt which is an area of high agricultural productivity. The intermediate domain (D02) has a horizontal resolution of 3 km and the innermost domain (D03) has a horizontal resolution of 1 km. Output from WRF-Chem is hourly for the D01 and D02 domains and 10-minutely from the D03 domain. WRF-Chem is run with 50 vertical levels. Initial and boundary conditions for the model come from the North American Regional Reanalysis (NARR). NARR has a 3-hourly temporal resolution, 32 km horizontal resolution, and a vertical resolution of 29 pressure levels (Mesinger et al. 2006). WRF-Chem utilizes the YSU Planetary Boundary Layer (PBL) scheme in all three domains and the Kain-Fritsch Cumulus Parameterization in D03 and D02 domains. An extended comparison of WRF-Chem meteorology to observations can be found in Martin et al. 2019.

Gridded mole fraction CO_2 data from CT-NRT are used as the initial and boundary conditions of atmospheric CO_2 concentrations for the WRF-Chem model. These data are considered as the model "background" because the data provides the base

atmospheric CO_2 state for WRF-Chem as well as the transport of CO_2 into the outer

WRF-Chem domain. A full list of the input data used to run WRF-Chem is provided in

Table 4.

Table 4. *Input data used to run WRF-Chem.*

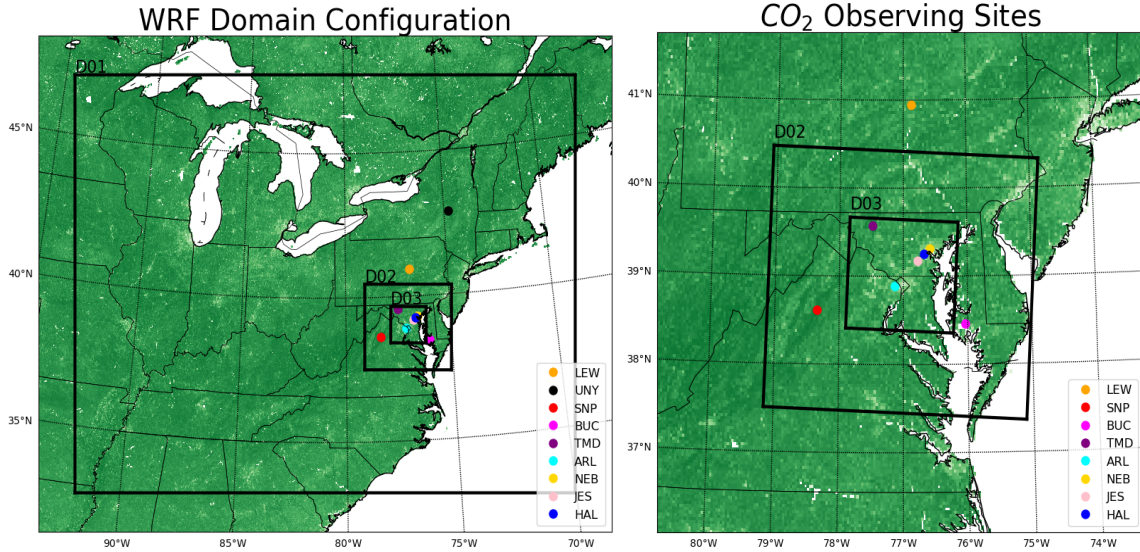| Input Data	Dataset	Horizontal Resolution	Temporal Resolution	Citation
Meteorological IC/BC	NARR	~ 0.3° x 0.3°	3-hourly	(Mesinger et al. 2006)
Atmospheric CO_2 IC/BC	CT-NRT	1.0° x 1.0°	3-hourly	(Peters et al. 2007)
Anthropogenic CO_2 Fluxes	FFDAS	0.1° x 0.1°	Hourly	(Rayner et al. 2010)
Biological Fluxes	VEGAS	2.5° x 2.5°	Hourly	-

Figure 1. *(left) A map of the WRF-Chem domain configuration and CO_2 observing sites used to compare against the WRF-Chem results. The D01 domain is modeled with a horizontal resolution of 9 km, the D02 domain is modeled with a 3 km resolution, and the D01 domain is modeled with a 1 km resolution. (right) A map of the WRF-Chem domains and the CO_2 monitoring sites over the immediate Baltimore/Washington region.*

Three tracer experiments are performed in the WRF-Chem modeling framework

and compared to observations at each of the NEC-B/W sites within the modeling domain.

The variable *F* denotes flux and the subscript denotes the type of flux. These experiments

include:

$$[CO_{2_{Anth}}] = F(CO_2)_{CT-NRT} + F(CO_2)_{FFDAS} \quad (2)$$
$$[CO_{2_{Bio}}] = F(CO_2)_{CT-NRT} + F(CO_2)_{VEGAS} \quad (3)$$
$$[CO_{2_{Total}}] = F(CO_2)_{CT-NRT} + F(CO_2)_{VEGAS} + F(CO_2)_{FFDAS} \quad (4)$$

These tracers allow for a direct comparison of the impact of anthropogenic emissions and uptake from the biosphere on atmospheric CO_2 concentrations. The WRF-Chem tracers are compared to the NIST tower observations from Table 1/Figure 1. Time series data of $CO_{2_{Total}}$ are extracted from WRF-Chem at the latitude, longitude, and height of each tower for comparisons of the model to observations. WRF-Chem mean bias from observations and standard error statistics are calculated for the $CO_{2_{Total}}$ data for the entirety of the model simulation as well as for the daytime and nighttime hours.

Wind speed and wind direction observations from the Cambrige-Dorchester Regional Airport (KCGE Latitude: 38.5393; Longitude: -76.0304) and Carroll County Regional Airport (KDMW Latitude: 39.6083; Longitude: -77.0077) AWOS stations are compared against WRF-Chem simulated wind speed and direction at the BUC and TMD CO_2 observing sites. Wind speed is converted to m/s to compare against model-simulated wind speed.

Lastly, VEGAS fluxes and FFDAS fluxes are averaged spatially and diurnally for D03 over the WRF-Chem period. This provides some insight into the contribution of VEGAS to the carbon cycle in the D01 domain and also provides some explanation for the WRF-Chem tracer experiment results.

Chapter 4. Results

This chapter presents the results of the 2 modeling experiments described in Chapter 3. Section 4.1 is where VEGAS output is validated against observations and the CT-NRT product. In Section 4.2, the results from the WRF-Chem experiment and validation are explained.

4.1 VEGAS Validation

4.1.1 Seasonal Variability

Domain averaged NEP from VEGAS is compared to domain averaged NDVI for D01 to study the onset and duration of the growing season. NEP is aggregated from hourly to daily averages to remove noise and for easier comparison to the weekly NDVI data. The averages are shown in Figure 2. This comparison reveals that VEGAS simulates a peak in biological productivity about a month earlier than in the VIIRS NDVI data and with a shorter growing season. Peak uptake in July is consistent with other vegetation carbon models (Raczka et al. 2013). NEP from VEGAS is above 75% of the max uptake (1.83 μmol m^2 s^{-1}), barring one day at the beginning of July, starting in mid-May and remains above 75% until early August. NDVI is above 75% of max NDVI (0.6) from the beginning of June through the beginning of October. Biological productivity decreases rapidly in mid-August in the VEGAS runs whereas NDVI appears to show a gradual decline as summer transitions to fall. The reason for this sharp decline is due to the biological processes in VEGAS. Once crops reach their maximum height, they are harvested and thus biological productivity is shut down. The same process is used for broadleaf trees. Once the conditions are met for dormancy, the trees drop their leaves and

cease carbon uptake. Because the D01 domain comprises mostly of cropland and broadleaf trees, the D01 averaged NEP is driven by these two processes.
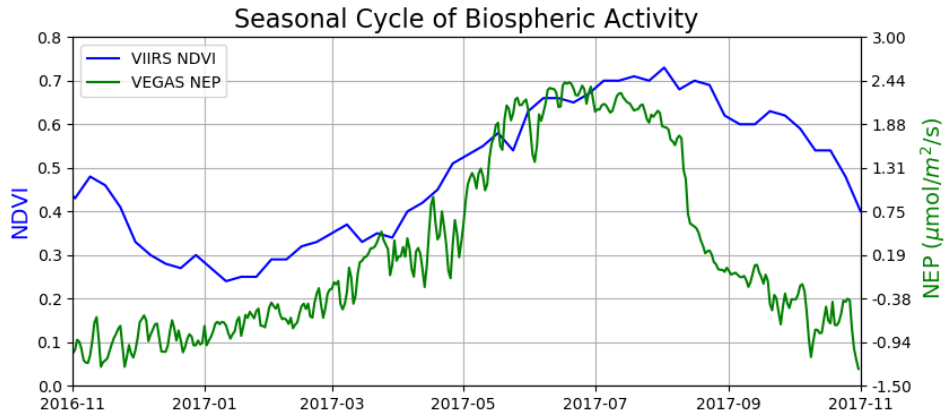

Figure 2. *Spatially averaged NDVI from VIIRS (blue) and NEP output from VEGAS (green) for the D01 domain.*

Fluxes from VEGAS are compared to CT-NRT for July 2017 in Figure 3. The July 2017 D01 mean NEE from VEGAS is -2.31 μmol m^2 s^{-1} while the D01 mean NEE for CT-NRT is -2.33 μmol m^2 s^{-1}. The monthly averaged maps reveal that VEGAS accurately captures the same spatial structure of NEE in D01 for July 2017 as the bio flux in CT-NRT. Areas of strong uptake include the Corn Belt with maximum uptake over Illinois and Central Iowa. Another area of high biological productivity from agriculture, which is simulated by VEGAS, is the area around Lake Ontario. This region is known for high agricultural productivity with the main crops being hay, corn, and soybeans. Because of the coarse resolution of VEGAS, the model is simulating the pixel over the water as agriculture. This matches with CT-NRT but is stronger in the VEGAS simulation. Because of the spatial resolution differences between VIIRS NDVI and VEGAS, it is difficult to perform spatial comparisons. As mentioned previously, NDVI is above 75% of its max by July 2017. Spatial plots of mean NDVI for July 2017 show that the biosphere is active for the D01 domain.
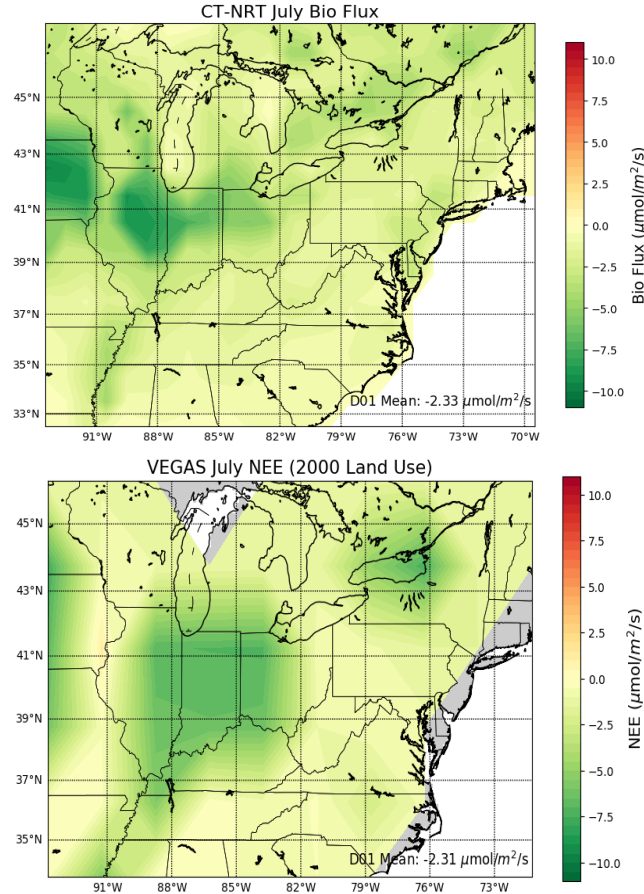
Figure 3. *Average July 2017 biosphere fluxes from the (top) CT-NRT product and (bottom) VEGAS. CT-NRT has a horizontal resolution of 1° x 1° while VEGAS has a horizontal resolution of 2.5° x 2.5°.*

4.1.2 Diurnal Variability

Diurnal comparisons in Figure 4 of D01 averaged NEE from VEGAS show that the diurnal scale is weaker than that in CT-NRT. Nighttime respiration in VEGAS is about half of that from CT-NRT while daytime uptake is slightly less than half. Uptake in VEGAS is consistent between days whereas the diurnal cycle is more variable in the CT-NRT product. Spatial comparisons of average fluxes at 1Z, 7Z, 13Z and 19Z show similar results. These time periods are chosen to match with the timestamps of the CT-NRT product. Peak uptake in VEGAS is 51% of that from CT-NRT. Peak respiration occurs at 1Z in CT-NRT while in VEGAS, peak respiration is at 7Z. Respiration in VEGAS is 48% of that from CT-NRT. As expected, the areas of peak uptake in the two

24

models are centered in the Corn Belt and up through Southern Ontario. These areas also match with peak respiration at night for CT-NRT. This is not the case in VEGAS. Areas of highest respiration in VEGAS are predominantly covered in the broadleaf PFT while the cropland PFT has the lowest respiration. Because the model has one PFT for cropland, average photosynthetic properties are estimated for maize, wheat, and rice. This simplification may be reducing the respiration from cropland.
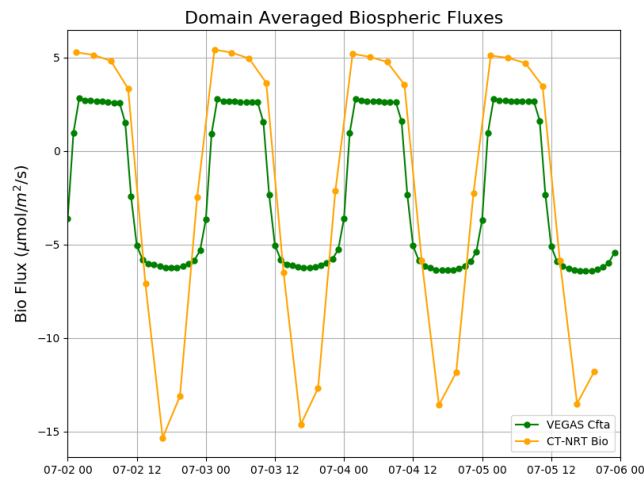

Figure 4. *Average biosphere fluxes for the D01 domain for the CT-NRT product (orange) and VEGAS (green). VEGAS has an hourly temporal resolution whereas CT-NRT has a 3-hourly temporal resolution.*

Diurnal uptake in VEGAS is compared to AmeriFlux observations in Figure 5 for the US-IB2 tower just outside of Chicago, IL. There are limitations when comparing a low-resolution model to point observations. Fluxes from VEGAS are expected to be smaller in magnitude than that of the productive meadow at US-IB2 because the fluxes are representative of the average biological productivity within the 2.5° x 2.5° grid cell. This is evident when comparing daily averaged fluxes from VEGAS to the observations. Interestingly, there is uptake in both the model and observations during early spring 2017. Observations from AmeriFlux show slight uptake in early March 2017 and VEGAS shows uptake beginning March 26, 2017. By the beginning of April 2017, VEGAS daytime uptake matches nighttime respiration on given days. Monthly averaged

maps of NDVI for the region over US-IB2 show low NDVI values in March 2017 with a considerable increase in NDVI by April 2017. For the grid cell where US-IB2 is located, NDVI increases from 0.27 to 0.47 from the beginning of March 2017 to the beginning of May 2017. Despite the inability of VEGAS to simulate the magnitude of the variability of the diurnal cycle of the US-IB2 station, the model does simulate daytime biological uptake early in the year.
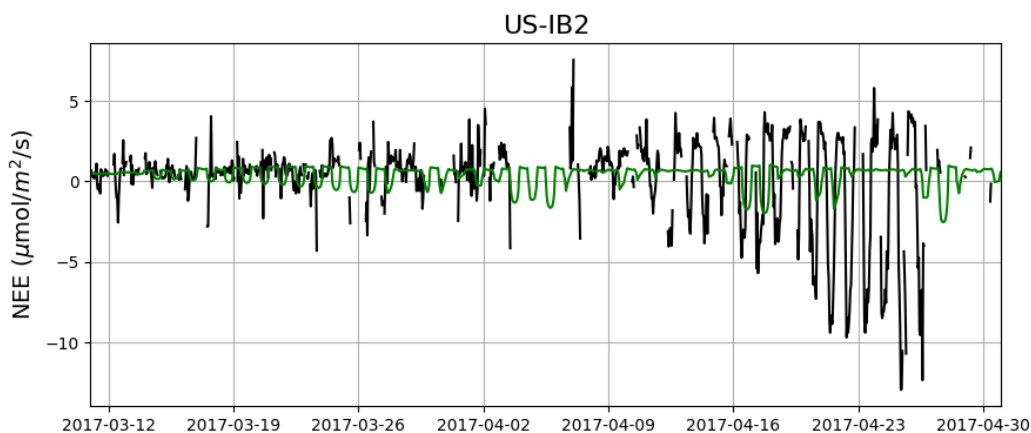

Figure 5. *Hourly flux tower measurements of NEE for the US-IB2 tower site (black) compared to the hourly VEGAS output of NEE for the grid cell location of the US-IB2 tower (green).*

4.2 WRF-Chem Comparisons

4.2.1 Background Tower Comparisons

Fluxes from the biosphere have a minor impact on the $CO_{2_{Total}}$ concentrations in the WRF-Chem simulation. This is evident through WRF-Chem comparisons to observations at the background tower sites. Background tower comparisons are performed for the two outer domains: D01: LEW and UNY as well as D02: SNP, BUC, and TMD. For the two D01 sites, the model over-predicts daytime $CO_{2_{Total}}$. The LEW site over-predicts daytime $CO_{2_{Total}}$ by 4.87 ppm and the UNY site over-predicts daytime $CO_{2_{Total}}$ by 5.79 ppm (Figure 6 and Figure 7). At both sites, WRF-Chem simulates very low variability in $CO_{2_{Bio}}$. In these rural areas, the model is unable to simulate high CO_2

26

uptake from the biosphere during the daytime. Further analysis of other D01 site

comparisons also show low variability in $CO_{2\,Bio}$ and $CO_{2\,Anth}$ for both daytime and

nighttime hours. This could be a result of the lower spatial resolution of 9 km in the D01

domain. The coarse resolution may be preventing the model from properly dispersing the

CO_2 tracers leading to low variability in those tracers in WRF-Chem at the observation

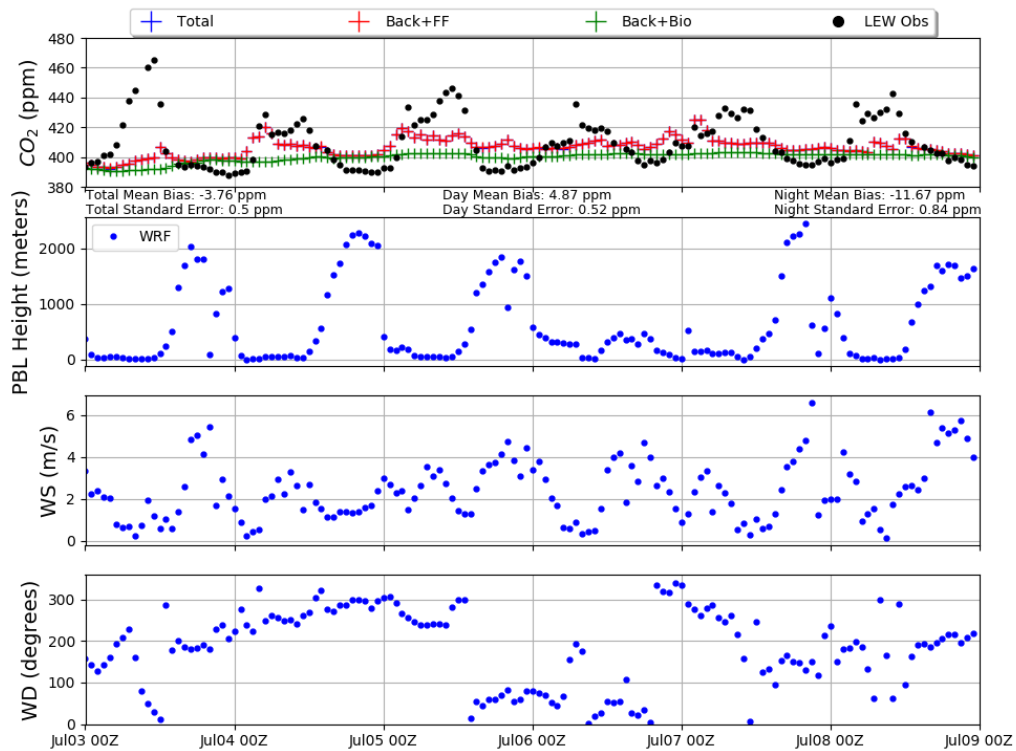site locations.

Figure 6. *(top) WRF-Chem CO_2 concentration for the three tracer experiments compared to the CO_2 observations for the LEW tower site. The bottom three panels show meteorological variables from the WRF-Chem simulation.*

Figure 7. *(top) WRF-Chem CO_2 concentration for the three tracer experiments compared to the CO_2 observations for the UNY tower site. The bottom three panels show meteorological variables from the WRF-Chem simulation.*

Observations at SNP in D02 show that the model is over predicting $CO_{2_{Total}}$ by 10 to 20 ppm during the day (Figure 8). This is the only station where the nighttime mean bias is lower than the daytime mean bias for D02. Complex meteorology due to the Blue Ridge Mountains, such as stronger vertical transport from orographic lifting, is likely to blame for the inability of WRF-Chem to match the observations at SNP.

Figure 8. *(top) WRF-Chem CO_2 concentration for the three tracer experiments compared to the CO_2 observations for the SNP tower site. The bottom three panels show meteorological variables from the WRF-Chem simulation.*
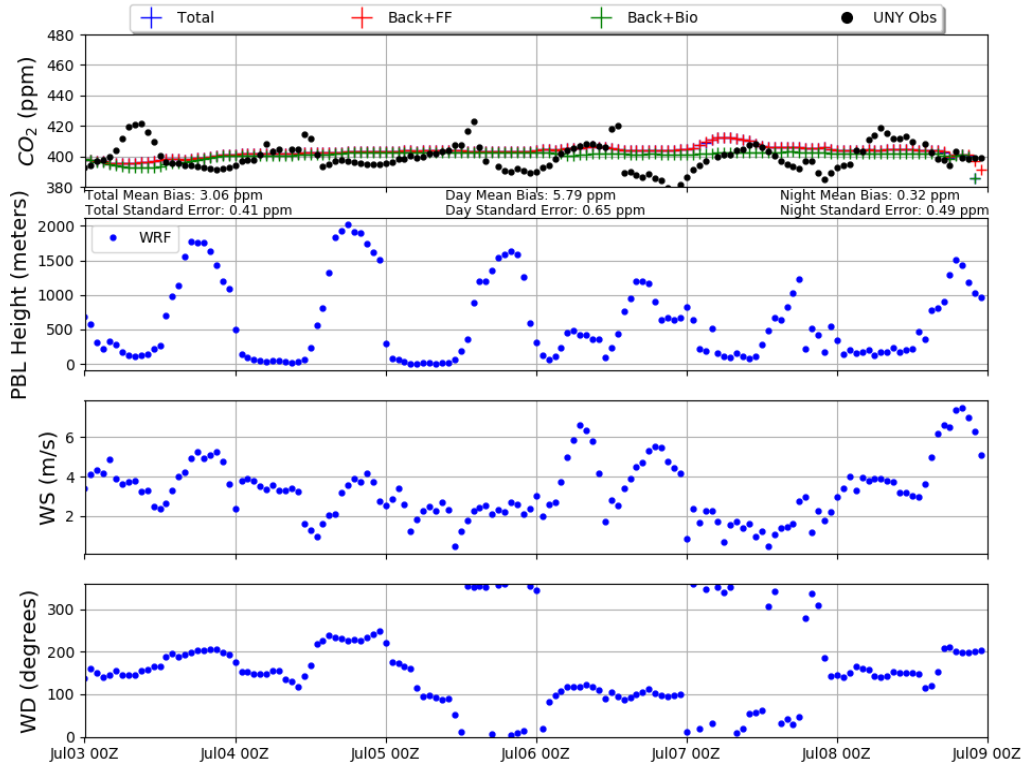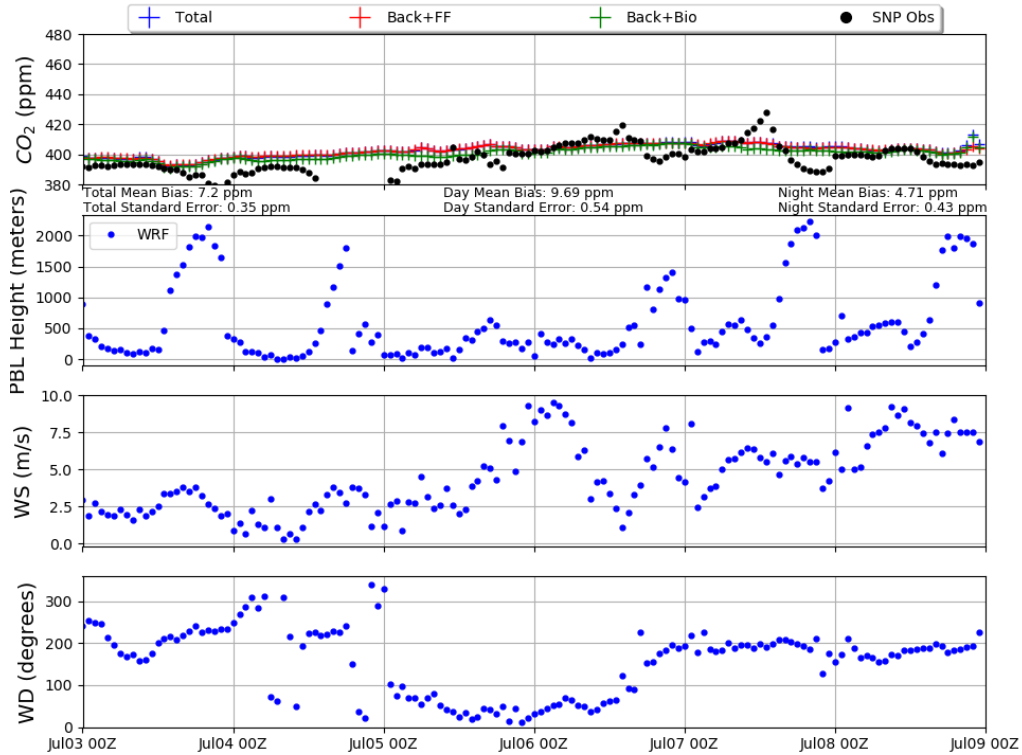
Comparisons at BUC in Figure 9 also show that the model over-predicts daytime $CO_{2_{Total}}$ by 2.19 ppm with differences as high as 20 ppm. TMD comparisons show a similar result with the model overestimates daytime concentrations by 3.6 ppm (Figure 10). WRF-Chem is over-predicting daytime CO_2 by as much as 13 ppm. Because the station is rural, anthropogenic emissions are believed to not affect the overall CO_2 concentration. As a result, variability in $CO_{2_{Total}}$ is expected to be driven mainly by the diurnal cycle of biological fluxes. This does not appear to be the case for $CO_{2_{Total}}$ at the BUC and TMD sites. Variability in $CO_{2_{Total}}$ is about 10 to 15 ppm while observations at both sites show variability of about 10 to 20 ppm on the diurnal scale. In rural areas, uptake from VEGAS is less than the observations. The standard error is also low for the BUC and TMD stations because the variability in $CO_{2_{Total}}$ is low.

It is interesting to note that the model does not simulate nighttime peaks in $CO_{2_{Total}}$ at BUC and TMD even though there are peaks measured by the background sites. There are 2 reasons for this. First, because the diurnal cycle in vegetation fluxes from VEGAS is quite small, the model is likely underestimating nighttime respiration as well. There must be something else contributing to the differences because the nighttime differences are so large at both sites (around 40 ppm for BUC and around 15 ppm for TMD). The second explanation for the differences is associated with meteorological transport. Despite these towers being background towers, they are still close enough to the urban areas that they are measuring $CO_{2_{Anth}}$. One such analysis for citing towers for the NEC-B/W found that during July, winds are predominantly from the southwest and northwest (Mueller et al. 2018). Towers downwind of urban areas may be measuring $CO_{2_{Anth}}$ even if they are considered background towers. Comparing WRF-Chem wind speed and wind direction to nearby meteorological observations provides some insight into this theory. For the BUC site, WRF-Chem is simulating westerly winds on the night of July 3 while observations at KCGE are showing northerly winds. On the night of July 7, WRF-Chem simulates a shift in the wind from northerly to southwesterly at the BUC site while observations at KCGE show a shift from northerly to northwesterly. The inability of the model to simulate wind direction on those nights is important given the large emissions sources of Baltimore and I-95 to the north and northwest of the BUC tower. The nights of July 5 and 6 are when WRF-Chem underestimates $CO_{2_{Total}}$ at the TMD site. On those nights, the model is simulating northeasterly winds at the TMD site while observations at KDMW show winds are from the southeast. Baltimore is to the

southeast of BUC which may be the reason why the model does not properly simulate the

two peaks in $CO_{2_{Total}}$.

Figure 9. *(top) WRF-Chem CO_2 concentration for the three tracer experiments compared to the CO_2 observations for the BUC tower site. The bottom three panels show meteorological variables from the WRF-Chem simulation. This figure includes meteorological observations of wind speed (WS) and wind direction (WD) for the bottom 2 panels from the KCGE AWOS station which is the nearest AWOS station to the BUC site.*
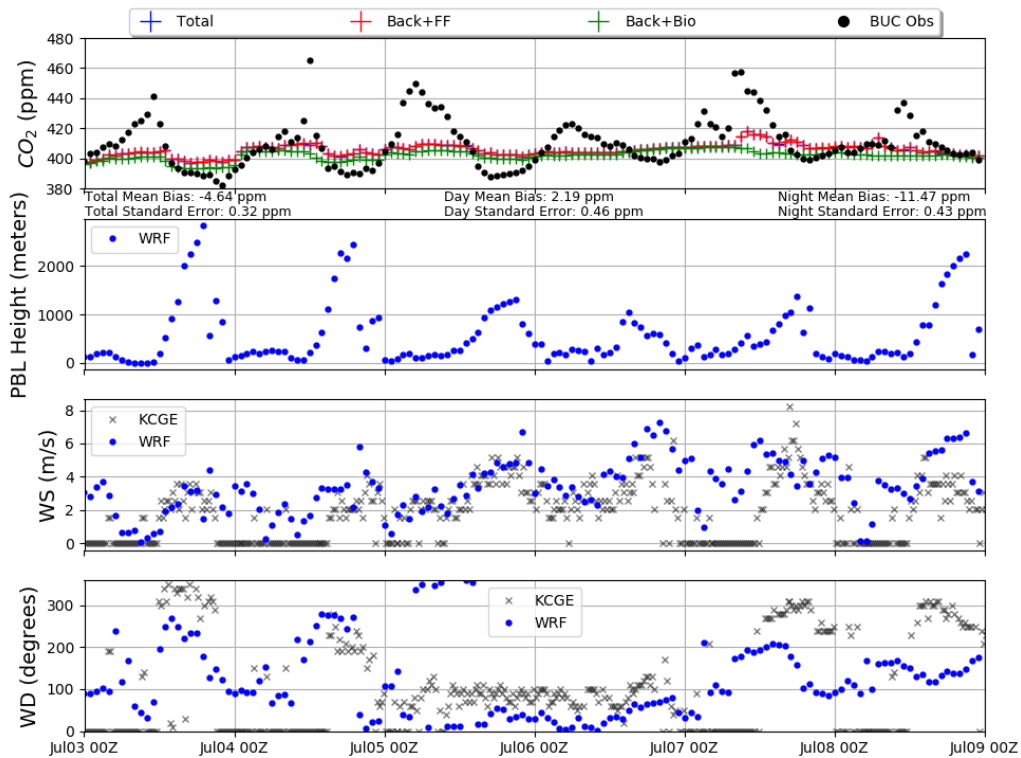
Figure 10. *WRF-Chem CO_2 concentration for the three tracer experiments compared to the CO_2 observations for the TMD tower site. The bottom three panels show meteorological variables from the WRF-Chem simulation. This figure includes meteorological observations of wind speed (WS) and wind direction (WD) for the bottom 2 panels from the KDMW AWOS station which is the nearest AWOS station to the TMD site.*
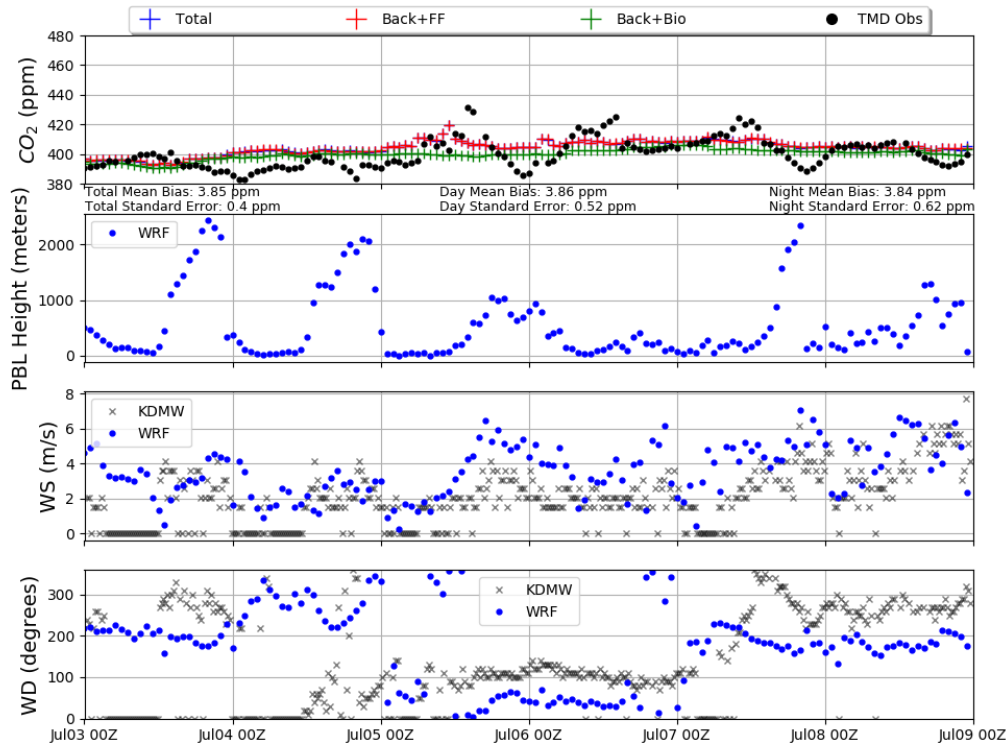
4.2.2 Urban Tower Comparisons

Across the 6 urban sites, half of the site comparisons have daytime mean biases that are lower than nighttime mean biases while the opposite is true for the other comparisons. The average daytime mean bias across all urban stations is 3.34 ppm with an average daytime standard error of 0.65 ppm. ARL has the lowest daytime mean bias of 1.68 ppm (Figure 11).
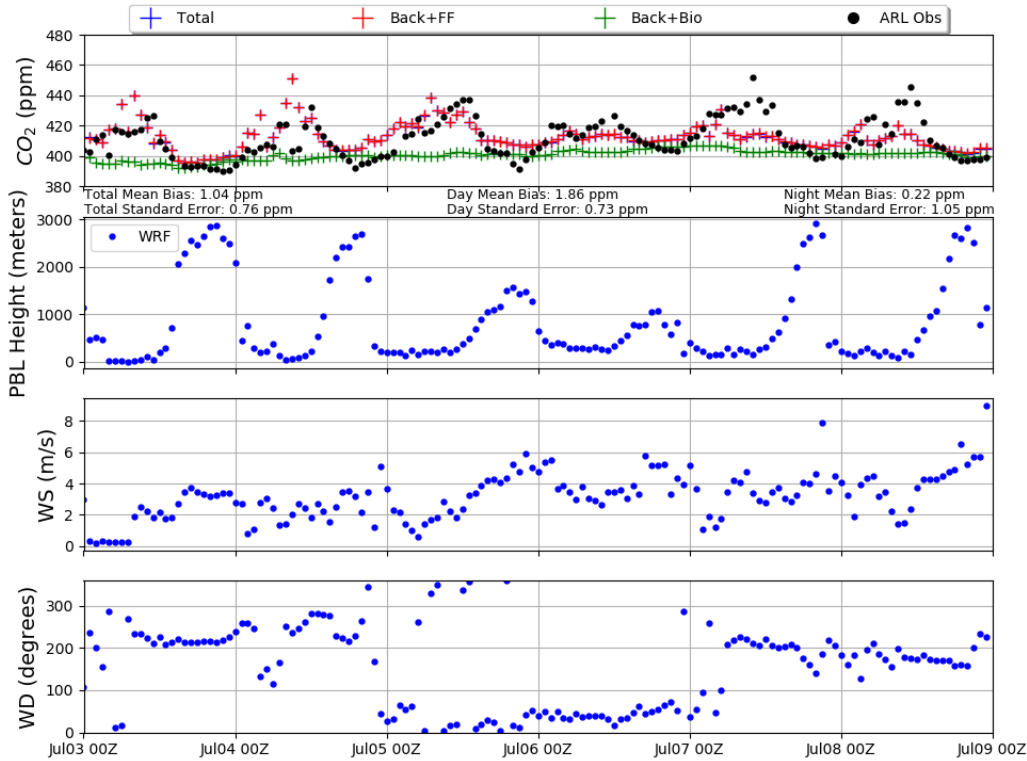
32

Figure 11. *(top) WRF-Chem CO_2 concentration for the three tracer experiments compared to the CO_2 observations for the ARL tower site. The bottom three panels show meteorological variables from the WRF-Chem simulation.*

ARL is to the west of Washington, DC. Winds are predominantly from the west during the simulation period so high concentration air from Washington, DC is not advected over the ARL observation tower. NEB has the highest daytime mean bias of 4.09 ppm (Figure 12). All station comparisons show a positive daytime mean bias compared to the observations with low variability in $CO_{2\,Bio}$. Stations such as JES, ARL, and HAL shows a weak diurnal cycle in $CO_{2\,Bio}$ of about 15-20 ppm on July 6 with an overall range of 390 ppm to 410 ppm during the simulation period.
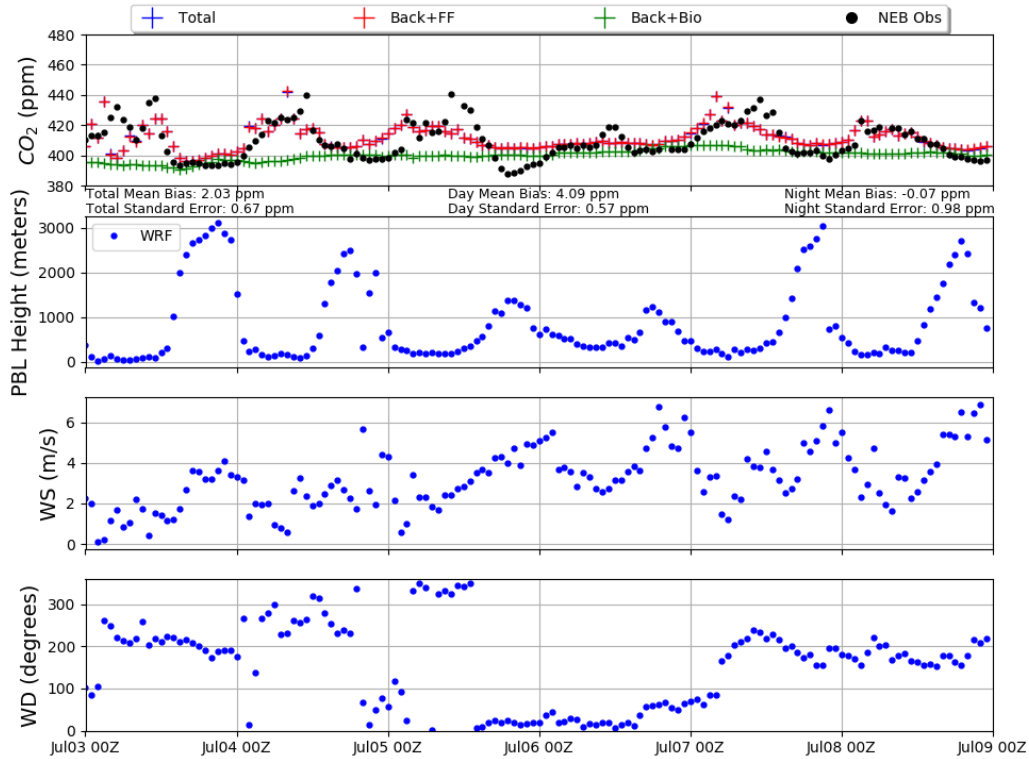
Figure 12. *(top) WRF-Chem CO$_2$ concentration for the three tracer experiments compared to the CO$_2$ observations for the NEB tower site. The bottom three panels show meteorological variables from the WRF-Chem simulation.*

Nighttime mean biases in CO$_{2\text{Total}}$ vary considerably across the stations. JES has the highest nighttime mean bias (Figure 13) of -8.83 ppm while NEB has the lowest nighttime mean bias of -0.07 ppm. Daytime and nighttime mean biases at HAL are comparable (Figure 14). Three stations have nighttime mean biases below 1 ppm while two other stations have nighttime mean biases below 5.4 ppm. Overall, WRF-Chem simulates the nighttime peak in CO$_{2\text{Total}}$ at the urban sites. These results are encouraging given that the biases are expected to be high at night because of the difficulty in modeling PBL height. At night, the PBL in the model collapses and traps CO$_2$ near the surface which leads to an overestimation of CO$_{2\text{Total}}$.
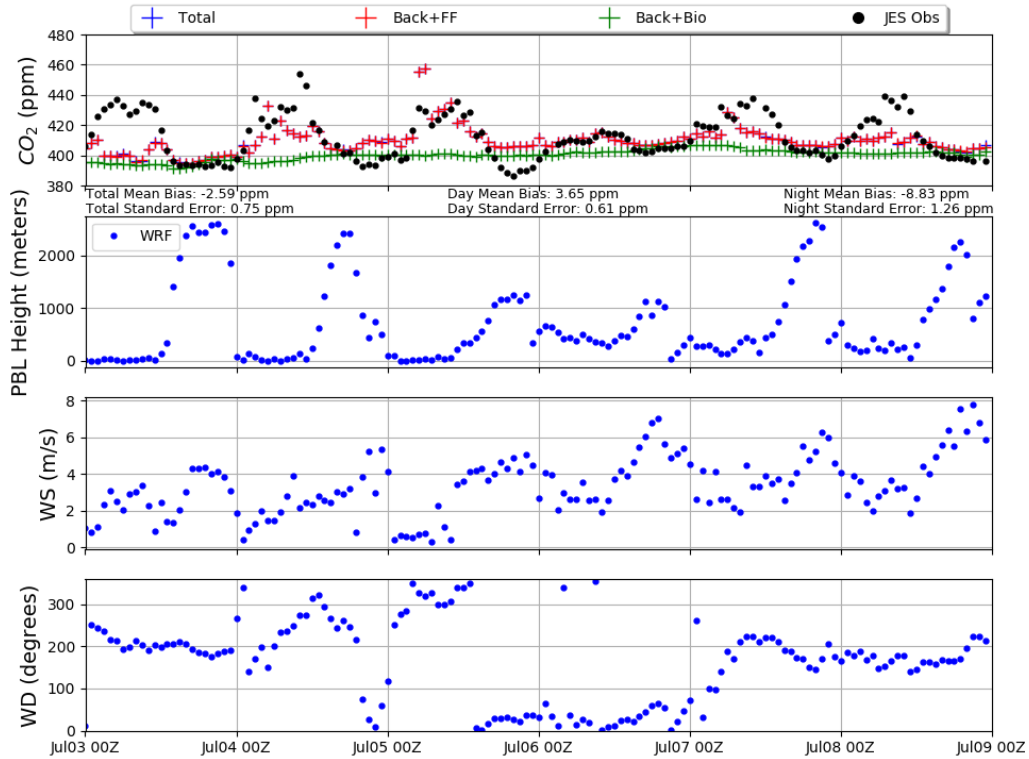
Figure 13. *(top) WRF-Chem CO_2 concentration for the three tracer experiments compared to the CO_2 observations for the JES tower site. The bottom three panels show meteorological variables from the WRF-Chem simulation.*

On the first three nights, the model simulates a PBL height of close to 0 m for the urban sites. The night of July 6, the model simulates the highest nighttime PBL of 500 m. Despite these low PBL heights, the model does capture the nighttime peaks in $CO_{2_{Total}}$. At NEB, the model has a slight time offset in the nighttime peak but simulates the mean CO_2 concentration well. When emissions are not dominant, the model does a poor job of simulating $CO_{2_{Total}}$ which resembles the result for the background stations. On July 6, emissions are low and thus variability is dominated by biological fluxes. This leads to an overestimation of CO_2 throughout the day and an overall decrease in the variability of $CO_{2_{Total}}$.
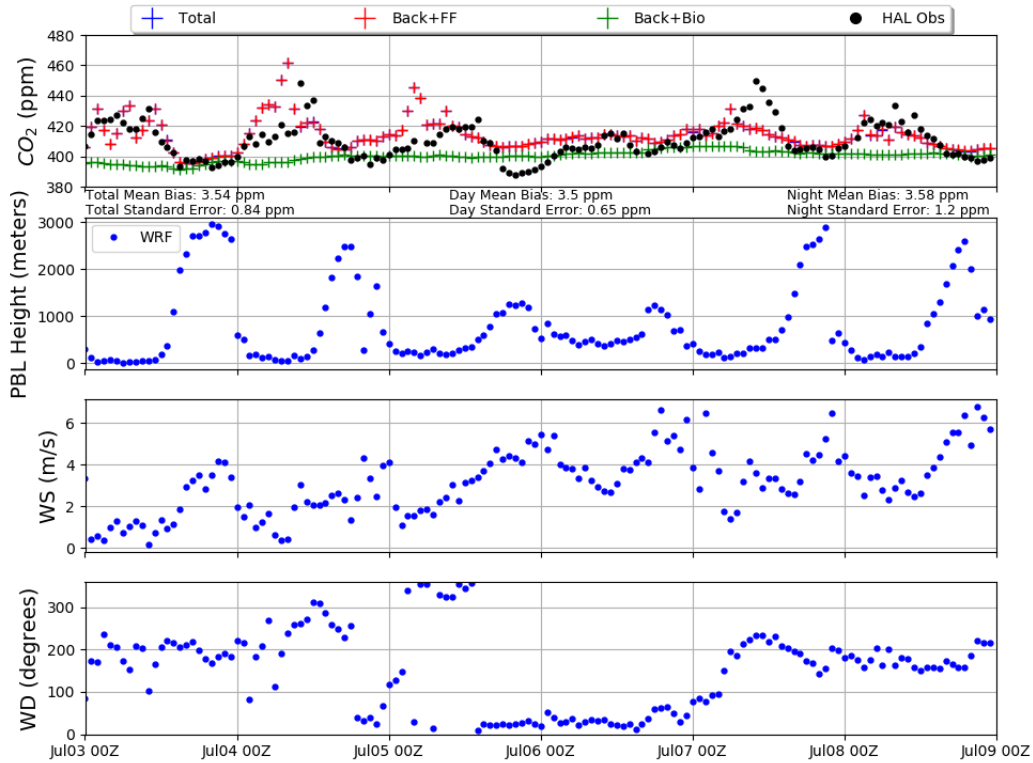
Figure 14. *(top) WRF-Chem CO_2 concentration for the three tracer experiments compared to the CO_2 observations for the HAL tower site. The bottom three panels show meteorological variables from the WRF-Chem simulation.*

4.2.3 CO_2 Flux Comparisons for the WRF-Chem Simulation

Further investigation of the fluxes in the D01 domain in early July 2017 reveals that VEGAS fluxes are a fraction of FFDAS emissions, summarized in Table 3. Mean biological fluxes from VEGAS account for the uptake of 32% of FFDAS emissions in D03 when averaged over the 6-day simulation period, which is much higher than the estimate in the introduction. This is important because the WRF-Chem results show that the model is not properly simulating $CO_{2_{Total}}$ during the daytime, meaning that fluxes at the diurnal scale do matter. VEGAS and FFDAS fluxes are averaged across the 6-day simulation period for 0Z, 6Z, 12Z, and 18Z. For the D01 domain, net emissions are positive throughout the entire day. Net fluxes are lower during the daytime hours (12Z and 18Z) because of the active biosphere while net fluxes are higher during nighttime

36

hours (0Z and 6Z) when primary productivity shuts down. VEGAS has a positive domain mean flux of 3.27 μmol m^{-2} s^{-1} at 6Z resulting from respiration. Respiration at night is on the order of magnitude of daytime peak uptake in the model.

Table 5. *D03 diurnally averaged fluxes for VEGAS and FFDAS. The VEGAS flux used is total biological flux (CFta). Averages are made for the instantaneous fluxes at the times listed above for the period of July 3, 2017 through July 9, 2017.*

Time (UTC)	VEGAS (μmol m^{-2} s^{-1})	FFDAS (μmol m^{-2} s^{-1})	FFDAS + VEGAS (μmol m^{-2} s^{-1})
0 Z	-0.559	3.991	3.432
6 Z	3.269	2.590	5.858
12 Z	-3.698	4.251	0.553
18 Z	-3.950	4.600	0.651
Mean	-1.235	3.858	2.624

Chapter 5. Summary and Conclusions

A dynamic vegetation model (VEGAS) was used with a chemical transport model (WRF-Chem) to estimate the influence of the biosphere in the carbon cycle in the Northeastern United States. VEGAS simulations were compared against satellite observations and other CO_2 analyses while WRF-Chem output was compared against CO_2 tower observations.

The results show that the growing season in VEGAS is shorter than the growing season in the NDVI measurements by about one month. This is a consequence of the simplified parameterizations within VEGAS which lead to an underrepresentation of biological uptake in the fall months in the model. VEGAS captures the spatial coverage of NEE and mean CO_2 sink for the D01 domain when compared to CT-NRT for the peak growing season in July 2017.

Despite the similarities in monthly averaged fluxes, the model differs from CT-NRT on the diurnal scale. VEGAS has a much smaller diurnal cycle than CT-NRT and does not simulate as strong of a daily peak in biological uptake. VEGAS has a much weaker diurnal cycle in NEE when compared to the US-IB2 AmeriFlux site. The model does simulate daytime biological uptake as early as March which is also measured by the US-IB2 site.

Across the 5 background sites, the biosphere leads to a roughly 10 to 15 ppm variability at some stations in the model domain but is largely underrepresented. WRF-Chem overestimates $CO_{2\,Total}$ for all of the background sites. Anthropogenic emissions are being measured at the BUC and TMD background sites but this is not represented in WRF-Chem because of model transport error.

For the urban sites, the model also over-predicts daytime $CO_{2_{Total}}$. Despite the suppressed diurnal cycle in VEGAS, WRF-Chem simulates nighttime CO_2 in urban areas. This result is surprising because of the poor representation of the PBL in this region within the model. The following conclusions can be made about the WRF-Chem framework used in this analysis: the model does well with representing CO_2 observations when anthropogenic emissions are high but underrepresents CO_2 observations when anthropogenic emissions are not the dominant source of variability.

Overall, VEGAS sequesters roughly 32% of FFDAS emissions in the D03 domain which is higher than 12% estimated at in the introduction. This means that properly simulating the diurnal fluxes is crucial to understanding the full carbon cycle on these scales.

To improve biological uptake in VEGAS, two changes must be made to the model. One reason that the model is not capturing the diurnal uptake is because of the low temporal resolution of the input temperature data which drives VEGAS. For this study, VEGAS is driven with 6-hourly CRUNCEP temperature data at 2 m. The low resolution prevents the model from simulating the sharp uptake which occurs as temperature peaks during the day in the growing season. A comparison of the current VEGAS simulation used in this study and a new experimental run driven by hourly temperature and radiation data is shown in Figure 15. GPP and CF_{ta} in the new simulation show more of a parabolic structure in uptake compared to the simulation used in this study which shows a plateau during the daytime hours. A new function for light dispersion within the canopy is also applied to VEGAS but does not improve the VEGAS simulation as drastically as the hourly driver data. Future improvements to the model

include assimilating observations from the biosphere of NDVI from satellite measurements or GPP from AmeriFlux sites to constrain the model. This approach will constrain the model using real observations and would thus nudge the model more towards the true biological state.
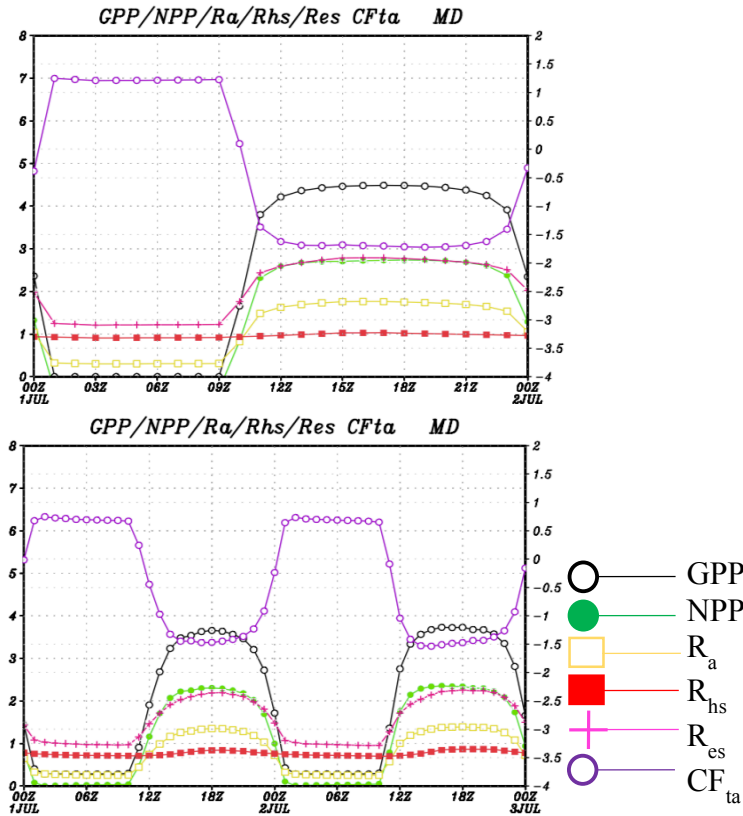

Figure 15. *(top) The diurnal cycle of biological fluxes at one grid cell over Maryland in early July for the VEGAS run used in this study. (bottom) The diurnal cycle for the same grid cell in Maryland from a new VEGAS run which utilizes hourly temperature and radiation data. This figure is meant to show how the new methods for running VEGAS are improving daytime uptake in the model. The simulations are for different years and should not be compared directly. R_{hs} is soil respiration. R_{es} is the total respiration (R_a + R_{hs}).*

References

Baldocchi, D., H. Chu, and M. Reichstein, 2018: Inter-annual variability of net and gross ecosystem carbon fluxes: A review. *Agric. For. Meteorol.*, **249**, 520–533, doi:10.1016/j.agrformet.2017.05.015. https://linkinghub.elsevier.com/retrieve/pii/S0168192317301806 (Accessed November 15, 2018).

Beck, V., T. Koch, R. Kretschmer, J. Marshall, R. Ahmadov, C. Gerbig, D. Pillai, and M. Heimann, 2011: *The WRF Greenhouse Gas Model (WRF-GHG) Technical Report*. Jena, Germany, https://www.bgc-jena.mpg.de/bgc-systems/pmwiki2/uploads/Download/Wrf-ghg/WRF-GHG_Techn_Report.pdf.

Bréon, F. M., and Coauthors, 2015: An attempt at estimating Paris area CO_2 emissions from atmospheric concentration measurements. *Atmos. Chem. Phys.*, **15**, 1707–1724, doi:10.5194/acp-15-1707-2015. https://www.atmos-chem-phys.net/15/1707/2015/.

Briber, B., and Coauthors, 2013: Variations in Atmospheric CO2 Mixing Ratios across a Boston, MA Urban to Rural Gradient. *Land*, **2**, 304–327, doi:10.3390/land2030304. http://www.mdpi.com/2073-445X/2/3/304.

Chen, M., P. Xie, J. E. Janowiak, P. A. Arkin, M. Chen, P. Xie, J. E. Janowiak, and P. A. Arkin, 2002: Global Land Precipitation: A 50-yr Monthly Analysis Based on Gauge Observations. *J. Hydrometeorol.*, **3**, 249–266, doi:10.1175/1525-7541(2002)003<0249:GLPAYM>2.0.CO;2. http://journals.ametsoc.org/doi/abs/10.1175/1525-7541%282002%29003%3C0249%3AGLPAYM%3E2.0.CO%3B2 (Accessed May 12, 2019).

Chevallier, F., and Coauthors, 2010: CO_2 surface fluxes at grid point scale estimated from a global 21 year reanalysis of atmospheric measurements. *J. Geophys. Res.*, **115**, D21307, doi:10.1029/2010JD013887. http://doi.wiley.com/10.1029/2010JD013887.

Collatz, G., M. Ribas-Carbo, and J. Berry, 1992: Coupled Photosynthesis-Stomatal Conductance Model for Leaves of C_4 Plants. *Aust. J. Plant Physiol.*, **19**, 519, doi:10.1071/PP9920519. http://www.publish.csiro.au/?paper=PP9920519.

Domke, G., and Coauthors, 2018: *Chapter 9: Forests. Second State of the Carbon Cycle Report*. Washington, DC, https://carbon2018.globalchange.gov/chapter/9/.

EPA, 2019: *Power Plant Emissions Trends*. https://www.epa.gov/airmarkets/power-plant-emission-trends.

FAA, 2017: *Automated Weather Observing Systems (AWOS) For Non-federal Applications*. 82 pp.

Feng, S., and Coauthors, 2016: Los Angeles megacity: a high-resolution land–atmosphere modelling system for urban CO_2 emissions. *Atmos. Chem. Phys.*, **16**, 9019–9045, doi:10.5194/acp-16-9019-2016. https://www.atmos-chem-phys.net/16/9019/2016/.

Grell, G. A., S. E. Peckham, R. Schmitz, S. A. McKeen, G. Frost, W. C. Skamarock, and B. Eder, 2005: Fully coupled "online" chemistry within the WRF model. *Atmos. Environ.*, **39**, 6957–6975, doi:10.1016/J.ATMOSENV.2005.04.027. https://www.sciencedirect.com/science/article/pii/S1352231005003560?via%3Dihub.

Gurney, K. R., D. Baker, P. Rayner, and S. Denning, 2008: Interannual variations in

continental-scale net carbon exchange and sensitivity to observing networks estimated from atmospheric CO_2 inversions for the period 1980 to 2005. *Global Biogeochem. Cycles*, **22**, n/a-n/a, doi:10.1029/2007GB003082. http://doi.wiley.com/10.1029/2007GB003082.

——, and Coauthors, 2017: Reconciling the differences between a bottom-up and inverse-estimated FFCO2 emissions estimate in a large US urban area. *Elem Sci Anth*, **5**, 44, doi:10.1525/elementa.137. https://www.elementascience.org/article/10.1525/elementa.137/.

Hulme, M., T. J. Osborn, and T. C. Johns, 1998: Precipitation sensitivity to global warming: Comparison of observations with HadCM2 simulations. *Geophys. Res. Lett.*, **25**, 3379–3382, doi:10.1029/98GL02562. http://doi.wiley.com/10.1029/98GL02562 (Accessed May 12, 2019).

Janowiak, J. E., P. Xie, J. E. Janowiak, and P. Xie, 1999: CAMS–OPI: A Global Satellite–Rain Gauge Merged Product for Real-Time Precipitation Monitoring Applications. *J. Clim.*, **12**, 3335–3342, doi:10.1175/1520-0442(1999)012<3335:COAGSR>2.0.CO;2. http://journals.ametsoc.org/doi/abs/10.1175/1520-0442%281999%29012%3C3335%3ACOAGSR%3E2.0.CO%3B2 (Accessed May 12, 2019).

Keeling, C. D., R. B. Bacastow, A. E. Bainbridge, C. A. Ekdahl, P. R. Guenther, L. S. Waterman, and J. F. S. Chin, 1976: Atmospheric carbon dioxide variations at Mauna Loa Observatory, Hawaii. *Tellus*, **28**, 538–551, doi:10.1111/j.2153-3490.1976.tb00701.x. http://tellusa.net/index.php/tellusa/article/view/11322.

Klein Goldewijk, K., A. Beusen, G. Van Drecht, and M. De Vos, 2011: The HYDE 3.1 spatially explicit database of human-induced global land-use change over the past 12,000 years. *Glob. Ecol. Biogeogr.*, **20**, 73–86, doi:10.1111/j.1466-8238.2010.00587.x. http://doi.wiley.com/10.1111/j.1466-8238.2010.00587.x (Accessed November 18, 2017).

Kogan, F., M. Goldberg, T. Schott, and W. Guo, 2015: Suomi NPP/VIIRS: improving drought watch, crop loss prediction, and food security. *Int. J. Remote Sens.*, **36**, 5373–5383, doi:10.1080/01431161.2015.1095370. http://www.tandfonline.com/doi/full/10.1080/01431161.2015.1095370 (Accessed September 12, 2018).

Kort, E. A., W. M. Angevine, R. Duren, and C. E. Miller, 2013: Surface observations for monitoring urban fossil fuel CO_2 emissions: Minimum site location requirements for the Los Angeles megacity. *J. Geophys. Res. Atmos.*, **118**, 1577–1584, doi:10.1002/jgrd.50135. http://doi.wiley.com/10.1002/jgrd.50135.

Lauvaux, T., and Coauthors, 2013: Urban Emissions of CO_2 from Davos, Switzerland: The First Real-Time Monitoring System Using an Atmospheric Inversion Technique. *J. Appl. Meteorol. Climatol.*, **52**, 2654–2668, doi:10.1175/JAMC-D-13-038.1. http://journals.ametsoc.org/doi/abs/10.1175/JAMC-D-13-038.1.

——, and Coauthors, 2016: High-resolution atmospheric inversion of urban CO_2 emissions during the dormant season of the Indianapolis Flux Experiment (INFLUX). *J. Geophys. Res. Atmos.*, **121**, 5213–5236, doi:10.1002/2015JD024473. http://doi.wiley.com/10.1002/2015JD024473.

Lopez-Coto, I., S. Ghosh, K. Prasad, and J. Whetstone, 2017: Tower-based greenhouse

gas measurement network design—The National Institute of Standards and Technology North East Corridor Testbed. *Adv. Atmos. Sci.*, **34**, 1095–1105, doi:10.1007/s00376-017-6094-6. http://link.springer.com/10.1007/s00376-017-6094-6 (Accessed April 7, 2019).

Maki, T., and Coauthors, 2010: New technique to analyse global distributions of CO_2 concentrations and fluxes from non-processed observational data. *Tellus B Chem. Phys. Meteorol.*, **62**, 797–809, doi:10.1111/j.1600-0889.2010.00488.x. https://www.tandfonline.com/doi/full/10.1111/j.1600-0889.2010.00488.x.

Martin, C. R., and Coauthors, 2019: Investigating sources of variability and error in simulations of carbon dioxide in an urban region. *Atmos. Environ.*, **199**, 55–69, doi:10.1016/j.atmosenv.2018.11.013. https://linkinghub.elsevier.com/retrieve/pii/S1352231018307799 (Accessed November 26, 2018).

Masarie, K. A., W. Peters, A. R. Jacobson, and P. P. Tans, 2014: ObsPack: a framework for the preparation, delivery, and attribution of atmospheric greenhouse gas measurements. *Earth Syst. Sci. Data*, **6**, 375–384, doi:10.5194/essd-6-375-2014. https://www.earth-syst-sci-data.net/6/375/2014/.

Masson-Delmotte, V., and Coauthors, 2018: *Summary for Policymakers — Global Warming of 1.5 ^{o}C*. Geneva, Switzerland, 32 pp. https://www.ipcc.ch/sr15/chapter/summary-for-policy-makers/.

Matamala, R., AmeriFlux US-IB2 Fermi National Accelerator Laboratory- Batavia (Prairie site). doi:doi:10.17190/AMF/1246066.

Mesinger, F., and Coauthors, 2006: North American Regional Reanalysis. *Bull. Am. Meteorol. Soc.*, **87**, 343–360, doi:10.1175/BAMS-87-3-343. http://journals.ametsoc.org/doi/abs/10.1175/BAMS-87-3-343 (Accessed December 1, 2017).

Miles, N. L., and Coauthors, 2017: Quantification of urban atmospheric boundary layer greenhouse gas dry mole fraction enhancements in the dormant season: Results from the Indianapolis Flux Experiment (INFLUX). *Elem Sci Anth*, **5**, 27, doi:10.1525/elementa.127. http://www.elementascience.org/article/10.1525/elementa.127/.

Mueller, K., V. Yadav, I. Lopez-Coto, A. Karion, S. Gourdji, C. Martin, and J. Whetstone, 2018: Siting Background Towers to Characterize Incoming Air for Urban Greenhouse Gas Estimation: A Case Study in the Washington, DC/Baltimore Area. *J. Geophys. Res. Atmos.*, doi:10.1002/2017JD027364. http://doi.wiley.com/10.1002/2017JD027364 (Accessed March 23, 2018).

Niwa, Y., T. Machida, Y. Sawa, H. Matsueda, T. J. Schuck, C. A. M. Brenninkmeijer, R. Imasu, and M. Satoh, 2012: Imposing strong constraints on tropical terrestrial CO_2 fluxes using passenger aircraft based measurements. *J. Geophys. Res. Atmos.*, **117**, n/a-n/a, doi:10.1029/2012JD017474. http://doi.wiley.com/10.1029/2012JD017474

Patra, P. K., M. Ishizawa, S. Maksyutov, T. Nakazawa, and G. Inoue, 2005: Role of biomass burning and climate anomalies for land-atmosphere carbon fluxes based on inverse modeling of atmospheric CO_2. *Global Biogeochem. Cycles*, **19**, doi:10.1029/2004GB002258. http://doi.wiley.com/10.1029/2004GB002258.

Peters, W., and Coauthors, 2007: An atmospheric perspective on North American carbon dioxide exchange: CarbonTracker. *Proc. Natl. Acad. Sci. U. S. A.*, **104**, 18925–

18930, doi:10.1073/pnas.0708986104.
http://www.ncbi.nlm.nih.gov/pubmed/18045791 (Accessed May 7, 2017).

Peylin, P., P. J. Rayner, P. Bousquet, C. Carouge, F. Hourdin, P. Heinrich, P. Ciais, and AEROCARB contributors, 2005: Daily CO_2 flux estimates over Europe from continuous atmospheric measurements: 1, inverse methodology. *Atmos. Chem. Phys.*, **5**, 3173–3186, doi:10.5194/acp-5-3173-2005. http://www.atmos-chem-phys.net/5/3173/2005/.

Potter, C. S., and S. A. Klooster, 1997: Global model estimates of carbon and nitrogen storage in litter and soil pools: response to changes in vegetation quality and biomass allocation. *Tellus B Chem. Phys. Meteorol.*, **49**, 1–17, doi:10.3402/tellusb.v49i1.15947. https://www.tandfonline.com/doi/full/10.3402/tellusb.v49i1.15947.

Raczka, B. M., and Coauthors, 2013: Evaluation of continental carbon cycle simulations with North American flux tower observations. *Ecol. Monogr.*, **83**, 531–556, doi:10.1890/12-0893.1. http://doi.wiley.com/10.1890/12-0893.1.

Rayner, P. J., R. M. Law, C. E. Allison, R. J. Francey, C. M. Trudinger, and C. Pickett-Heaps, 2008: Interannual variability of the global carbon cycle (1992-2005) inferred by inversion of atmospheric CO_2 and δ 13 CO_2 measurements. *Global Biogeochem. Cycles*, **22**, n/a-n/a, doi:10.1029/2007GB003068. http://doi.wiley.com/10.1029/2007GB00306.

——, M. R. Raupach, M. Paget, P. Peylin, and E. Koffi, 2010: A new global gridded data set of CO_2 emissions from fossil fuel combustion: Methodology and evaluation. *J. Geophys. Res.*, **115**, D19306, doi:10.1029/2009JD013439. http://doi.wiley.com/10.1029/2009JD013439.

Sargent, M., and Coauthors, 2018: Anthropogenic and biogenic CO2 fluxes in the Boston urban region. *Proc. Natl. Acad. Sci.*, **115**, 7491–7496, doi:10.1073/PNAS.1803715115. https://www.pnas.org/content/115/29/7491.short.

Sitch, S., and Coauthors, 2015: Recent trends and drivers of regional sources and sinks of carbon dioxide. *Biogeosciences*, **12**, 653–679, doi:10.5194/bg-12-653-2015. https://www.biogeosciences.net/12/653/2015/.

Skamarock, W. C., and Coauthors, 2008: *A Description of the Advanced Research WRF Version 3*. Boulder, CO, 125 pp.

Turnbull, J. C., and Coauthors, 2015: Toward quantification and source sector identification of fossil fuel CO_2 emissions from an urban area: Results from the INFLUX experiment. *J. Geophys. Res. Atmos.*, **120**, 292–312, doi:10.1002/2014JD022555. http://doi.wiley.com/10.1002/2014JD022555 (.

Verhulst, K. R., and Coauthors, 2017: Carbon dioxide and methane measurements from the Los Angeles Megacity Carbon Project – Part 1: calibration, urban enhancements, and uncertainty estimates. *Atmos. Chem. Phys.*, **17**, 8313–8341, doi:10.5194/acp-17-8313-2017. https://www.atmos-chem-phys.net/17/8313/2017/.

Viovy, N., 2019: CRUNCEP Version 9. https://vesg.ipsl.upmc.fr/thredds/catalog/work/p529viov/cruncep/V9_1901_2017/catalog.html (Accessed June 30, 2018).

Yang, W., F. Kogan, W. Guo, and Y. Chen, A Novel VCI Re-compositing Approach to Create a Continuous and Consistent Cross-Sensor Global NDVI Data Set. *Remote Sens. Environ.*,.

Zeng, N., A. Mariotti, and P. Wetzel, 2005: Terrestrial mechanisms of interannual CO_2 variability. *Global Biogeochem. Cycles*, **19**, doi:10.1029/2004GB002273. http://doi.wiley.com/10.1029/2004GB002273 (Accessed August 15, 2017).